Solar Hydrogen Production on Some Water Splitting Photocatalysts

Tsuyoshi Takata, Takashi Hisatomi, Kazunari Domen
Department of Chemical System Engineering, School of Engineering, The University of Tokyo,
7-3-1 Hongo Bunkyo-ku, 113-8656 Japan

ABSTRACT

Photocatalytic overall water splitting into H_2 and O_2 is expected to be a promising method for the efficient utilization of solar energy. The design of optimal photocatalyst structures is a key to efficient overall water splitting, and the development of photocatalysts which can efficiently convert large portion of visible light spectrum has been required. Recently, a series of complex perovskite type transition metal oxynitrides, $LaMg_xTa_{1-x}O_{1+3x}N_{2-3x}$, was developed as photocatalysts for direct water splitting operable at wide wavelength of visible light. In addition two-step excitation water splitting via a novel photocatalytic device termed as photocatalyst sheet was developed. This consists of two types of semiconductors (hydrogen evolution photocatalyst and oxygen evolution photocatalyst) particles embedded in a conductive layer, and showed high efficiency for overall water splitting. These recent advances in photocatalytic water splitting were introduced.

Keywords: Photocatalyst, semiconductor, water splitting, hydrogen, oxynitride, Z-scheme, photocatalyst sheet

INTRODUCTION

Water splitting into hydrogen and oxygen via photocatalysis is a fundamental process for photon-to-chemical energy conversion. The hydrogen generated by this process can subsequently be used for the catalytic fixation of carbon dioxide and nitrogen to generate hydrocarbons/alcohols and ammonia, respectively, which have applications as fuels and/or chemicals. One of the simplest methods of splitting water using solar energy is to use a particulate-type semiconductor photocatalyst with a suitable bandgap energy and position to evolve H_2 and O_2. This would also be expected to be the most scalable and cost-effective route for large-scale renewable hydrogen production[1]. Over the last several decades, remarkable progress has been made in semiconductor photocatalysts. Many UV-light-sensitive oxide photocatalysts have been developed to be capable of overall water splitting with high quantum efficiencies[2-6]. Recent effort has been devoted to develop a semiconductor photocatalyst which can efficiently convert wide wavelength range of visible light. Here we introduce recent advances in the study of photocatalytic water splitting with a main focus on the use of particulate-type semiconductors.

A COMPLEX PEROVSKITE OXYNITRIDE PHOTOCATALYST FOR DIRECT WATER SPLITTING UNDER VISIBLE LIGHT

Many (oxy)nitrides based on d^0- or d^{10}-metal cations have been carefully examined as photocatalysts for visible-light-driven water splitting. Among them a d^{10}-type oxynitride, $(Ga_{1-x}Zn_x)(N_{1-x}O_x)$, was first found to be capable of overall water splitting[7,8]. This material is a series of solid solutions between GaN and ZnO having a same crystal structure. While $(Ga_{1-x}Zn_x)(N_{1-x}O_x)$ can utilize visible light for overall water splitting, the usable wavelength of this material is limited to that under approximately 500 nm. Therefore, this material can utilize a small portion of the sunlight spectrum, and further extension of usable wavelength is desirable in order to efficiently harness solar energy.

For this reason, the d^0-transition metal oxynitrides are preferable because they tend to have absorption edges above 600 nm[8-11]. Initial surveys of the d^0-transition metal (oxy)nitrides found that none of these compounds realized overall water splitting. Then various new approaches have been attempts to improve the design of these potential photocatalysts, primarily focusing on modification of the bulk composition and developing techniques for advanced surface modification. With regard to the former approach, the incorporation of foreign metals into d^0-transition metal oxynitrides has been examined. Among the various combinations of parent (oxy)nitrides and foreign metal cations examined, $LaTaON_2$ incorporated with Mg was recently found to be active for water splitting, as detailed below[12-14].

Solar Hydrogen and Nanotechnology XI, edited by Chung-Li Dong, Proc. of SPIE Vol. 9935,
99350O · © 2016 SPIE · CCC code: 0277-786X/16/$18 · doi: 10.1117/12.2236434

$LaTaON_2$ has a perovskite structure[15]. La^{3+} and Ta^{5+} occupy so-called A and B sites in the perovskite structure, respectively. The ionic radius of Mg^{2+} is closer to that of Ta^{5+} rather than that of La^{3+}, and so selective Mg^{2+}/Ta^{5+} substitution is possible. In this case, O^{2-}/N^{3-} substitution concurrently occurs to maintain the charge balance as well as the original crystal structure, resulting in the formation of complex perovskites: $LaMg_xTa_{1-x}O_{1+3x}N_{2-3x}$ ($0 \leq x \leq 0.67$)[16]. These materials can be regarded as a series of solid solutions composed of the perovskite oxynitride $LaTaON_2$ and the perovskite oxide $LaMg_{2/3}Ta_{1/3}O_3$ [17] (Fig. 1).

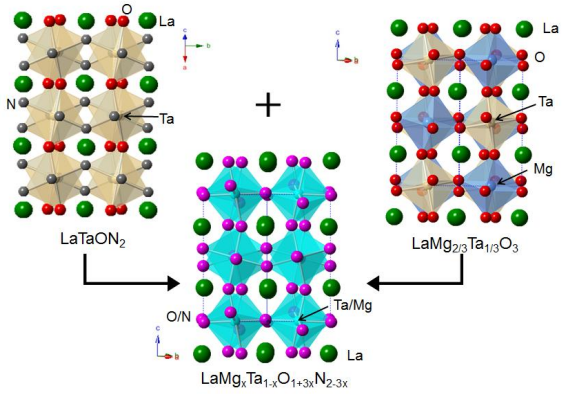

Fig. 1. Crystal structures of $LaMg_xTa_{1-x}O_{1+3x}N_{2-3x}$ solid solutions.

Incorporation of Mg in $LaTaON_2$ results in the change of optical absorption. The UV-vis spectra in Fig. 2 showed that the absorption band edge shifts to shorter wavelengths (from 640 to 520 nm) as x increases from 0 to 0.6, indicating bandgap widening from 1.93 to 2.38 eV. From density functional theory (DFT) study, a major change was found to occur in the VBM level upon incorporating Mg because of the change in the O/N ratio[14].

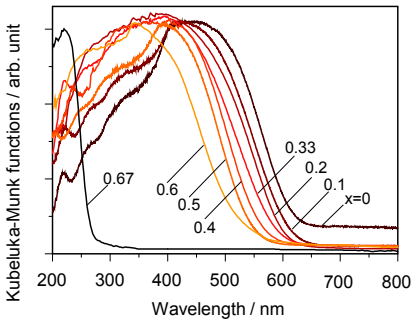

Fig. 2. UV-vis diffuse reflectance spectra of $LaMg_xTa_{1-x}O_{1+3x}N_{2-3x}$.

When $LaMg_xTa_{1-x}O_{1+3x}N_{2-3x}$ was combined with $RhCrO_y$ as a H_2 evolution cocatalyst, photocatalytic activity was observed at all compositions. The photocatalytic activity of the $LaMg_xTa_{1-x}O_{1+3x}N_{2-3x}$ series was found to vary with the Mg content. Among them, a composition of x = 1/3, $LaMg_{1/3}Ta_{2/3}O_2N$, showed better activity than others. Fig. 3 shows typical time course of gas evolution on $RhCrO_y/LaMg_{1/3}Ta_{2/3}O_2N$ during photoirradiation. H_2 and O_2 evolution was observed, but N_2 evolution also occurred continuously. The ratio of the produced amounts of H_2 and O_2 was diverged from the stoichiometry of water splitting. The observed N_2 evolution is attributed to the oxidation of nitrogen species on the surface of photocatalyst, namely, self-oxidation of the photocatalyst. This N_2 evolution was identically observed for the samples with different Mg concentrations. In addition, reverse reaction to regenerate water from the produced H_2 and O_2 appeared to occur as suggested from the decreased amount of the O_2 accumulation in the latter part of the irradiation duration. Therefore, N_2 evolution and reverse reaction were likely to be the main obstacles to realize overall water splitting. Then a novel surface modification was introduced to solve these problems mainly based on kinetic control as written below.

The entire surface of the photocatalyst particles was covered by some transition metal oxides via photodecomposition from their aqueous peroxide solutions[12,13]. Fig. 4 shows the typical time courses of gas evolution during an attempt at water splitting on Ta_2O_5-photodepositted $RhCrO_y/LaMg_{1/3}Ta_{2/3}O_2N$ under UV and visible light. H_2 and O_2 generated

upon photoirradiation with nearly 2:1 ratio, and N_2 evolution was almost prevented. Overall water splitting was also successful after photodepositing TiO_2, ZrO_2 or Nb_2O_5. Overall water splitting proceeded above x = 1/3 after these oxides deposition, and the sample with x = 1/3 showed the highest activity. Increasing Mg concentration shifts the VBM level toward positive potential, resulting in a concurrent increase in oxidation ability[14]. This is likely responsible for the successful overall water splitting above x = 1/3. Incorporation of Mg into the $LaTaON_2$ enlarges the bandgap energy, although the sample with x = 1/3 has an optical absorption band edge at approximately 600 nm and so still overlaps sufficiently with the sunlight spectrum. This is the first successful case of direct water splitting on a photocatalyst operable up to 600 nm.

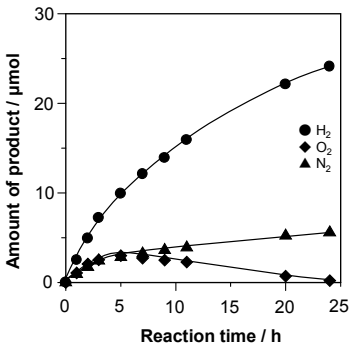

Fig. 3. Time courses of gas evolution during attempt at water splitting on $RhCrO_x/LaMg_{1/3}Ta_{2/3}O_2N$. Catalyst: 0.1 g, solvent: 250 mL H_2O, light source: Xe lamp (300 W, $\lambda \geq 300$ nm).

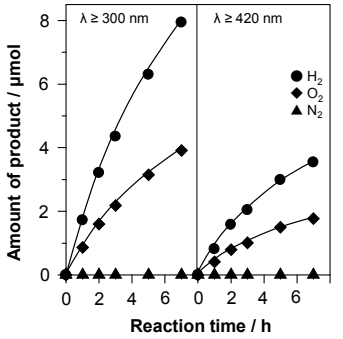

Fig. 4. Time courses of gas evolution during attempt at water splitting on $Ta_2O_5/RhCrO_x/LaMg_{1/3}Ta_{2/3}O_2N$. Catalyst: 0.1 g, solvent: 250 mL H_2O, light source: Xe lamp (300 W).

The coating oxides existed as amorphous and hydrous forms. In this case, the reactant water molecules can be incorporated into the coating layer by hydration and are thus able to reach the interface between the semiconductor photocatalyst and coating layer. The H_2 and O_2 produced by water splitting can be released by permeation through the coating layer while the released H_2 and O_2 are unable to diffuse back into the coating layer because they are less polar molecules and have less affinity for the coating material. This selective permeability prevents the access of product molecules to the active sites for the reverse reaction, while simultaneously allowing reactant molecules to reach the reaction sites. Thus, the reverse reaction can be prevented without suppressing the water splitting process, leading to successful overall water splitting (Fig. 5)[18].

Presently, the highest quantum efficiency obtained from this type of photocatalyst is on the order of 0.2% at 440 nm, and so further enhancement is required to sufficiently harness solar energy. Since the requirements for overall water splitting on a single-type particulate photocatalyst are relatively demanding, improved systems are necessary in addition

to better photocatalytic materials. In any event, the approaches described above are important and indispensable steps toward achieving practical water splitting systems.

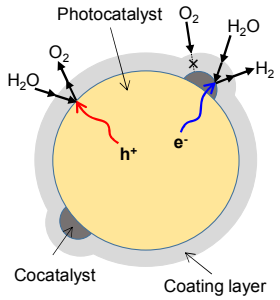

Fig. 5. Reaction mechanism for overall water splitting on a surface-coated photocatalyst.

PHOTOCATALYST SHEET DEVICES FOR TWO-STEP EXCITATION WATER SPLITTING

In the previous section, photocatalytic water splitting using a single semiconductor photocatalyst, primarily $LaMg_{1/3}Ta_{2/3}O_2N$, is considered. However, the apparent quantum efficiency is still low even though visible light of up to 600 nm has become available. This suggests a difficulty of one-step excitation overall water spitting using narrow bandgap semiconductor photocatalysts likely due to small voltages applicable to water splitting. Water splitting by two-step excitation, commonly termed as Z-scheme, is suited for harvesting of long-wavelength light, because narrow bandgap photocatalysts that only have potential to evolve either H_2 or O_2 can be applied as a hydrogen evolution photocatalyst (HEP) or an oxygen evolution photocatalyst (OEP), respectively, to split water in Z-scheme systems as shown in Fig. 6. In this scheme, electrons in the HEP and holes in the OEP are used to evolve H_2 and O_2, respectively, and remaining charges recombine via reversible reactions of redox couples or interparticle electron transfer[19].

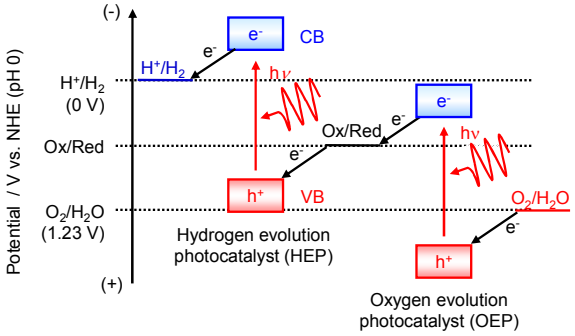

Fig. 6. Energy diagram of Z-scheme water splitting based on two-step excitation. HEP, OEP, CB and VB stand for hydrogen evolution photocatalyst, oxygen evolution photocatalyst, conduction band and valence band, respectively.

Z-scheme water splitting can be accomplished when a HEP and an OEP are suspended in an aqueous solution containing appropriate redox couples such as IO_3^-/I^-, Fe^{3+}/Fe^{2+}, and $[Co(bpy)_3]^{3+/2+}$ [20-24]. However, reactions of redox couples are thermodynamically more favourable and therefore tend to proceed more readily than the H_2 and O_2 evolution reactions. No water splitting may occur when reduction (oxidation) of redox couples proceeds predominantly instead of H_2 (O_2) evolution. In addition, some redox couples absorb visible light and shade photocatalyst particles from incident light. Therefore, it is generally necessary to apply appropriate species and concentrations of redox couples depending on adsorption properties and reactivity of the photocatalysts employed in order to ensure the best performance. To avoid problems arising from the use of redox couples, Z-scheme systems based on interparticle electron transfer in the absence of redox couples have been studied[25,26]. HEP and OEP particles suspended in an aqueous solution can be charged in the opposite signs when pH of the solution is between the zero charge points of the respective photocatalysts[25]. Under such conditions, the HEP and OEP particles can form aggregates by electrostatic attractive force and have opportunities for interparticle electron transfer. However, kinds of photocatalysts and reaction solutions applicable to this type of Z-

scheme water splitting are quite limited. In addition, the efficiency of the interparticles electron transfer is generally low because it occurs across photocatalyst particles that are just physically adsorbed onto each other. Alternatively, it has also been studied forming composites of HEP and OEP by preparing one photocatalyst in the presence of the other[27]. However, photocatalyst materials that can be applicable to this concept is also limited because the preparation conditions for different photocatalyst materials are incompatible in most cases.

Recently, photocatalyst sheets[28] based on HEP and OEP particles embedded into a conductive layer by particle transfer[29] has been devised to overcome the aforementioned problems of the conventional Z-scheme systems. The particle transfer method was originally developed to prepare composites of particulate photocatalysts and conductive layers with excellent mechanical and electrical contacts for application as photoelectrodes[28]. The general preparation scheme of photocatalyst sheets for Z-scheme water splitting by particle transfer is presented in Fig. 7. Firstly, a mixture of HEP and OEP particles are deposited on a substrate. Subsequently, a conductive material is deposited over the photocatalyst particle layer. Then, the composite of photocatalysts and conductive layer is peeled off with an adhesive tape supported by another substrate. Finally, the sample is ultrasonicated to remove photocatalyst particles that are not embedded into the conductive layer but just physically attached onto other photocatalyst particles. Using this process, composites of HEP and OEP particles embedded into a conductive layer without a significant grain boundary resistance can be obtained and used as photocatalyst sheets. Notably, this process is applicable to various particulate semiconductor and conductor materials regardless of their surface properties or reactivity[28].

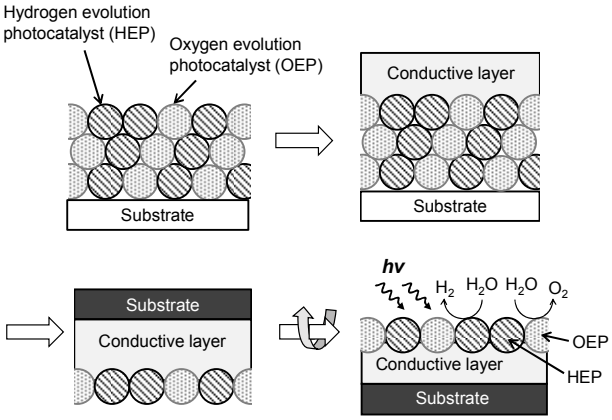

Fig. 7. Schematic of general preparation process for photocatalyst sheets.

One example of photocatalyst sheets applicable to Z-scheme water splitting is a system consisting of La- and Rh-codoped $SrTiO_3$ ($SrTiO_3$:La,Rh) as the HEP, $BiVO_4$ as the OEP, and Au as the conductive layer[28]. $SrTiO_3$:La,Rh evolves H_2 under irradiation of up to ca. 520 nm from aqueous solution containing an electron donor (*e.g.*, methanol) when it is modified with an appropriate H_2 evolution cocatalyst, while $BiVO_4$ evolves O_2 from an aqueous solution containing an electron acceptor (*e.g.*, silver ion) under irradiation of up to 540 nm. Fig. 8 shows time courses of gas evolution during the Z-scheme water splitting using photocatalyst sheets and powder suspension consisting of $SrTiO_3$:La,Rh and $BiVO_4$ under visible light ($\lambda > 420$ nm) after loading of a Ru cocatalyst by photodeposition. The photocatalyst powder suspension is active in the Z-scheme water splitting reaction owing to interparticle electron transfer. The photocatalyst sheet without a conductive layer, which consists of HEP and OEP powders fixed on an adhesive tape, shows a lower water splitting rate because the contact between HEP and OEP particles are restricted. In contrast, the photocatalyst sheet with a conductive layer showed a more than five times higher water splitting rate than the powder suspension. This result clearly indicates that the Au layer effectively promotes electron transfer between the HEP and OEP particles and thereby enhances Z-scheme water splitting. The solar-to-hydrogen energy conversion efficiency (STH) and the apparent quantum efficiency at 420 nm of this system are 0.2% and 5.9%, respectively. Moreover, the STH has been recently increased to more than 1.0% through optimization of photocatalyst sheet preparation and water splitting reaction conditions[30]. This STH is by far the highest among the water splitting systems based on particulate photocatalysts. The photocatalyst sheet system has significant potential to enhance the activity of particulate photocatalysts in Z-scheme water splitting.

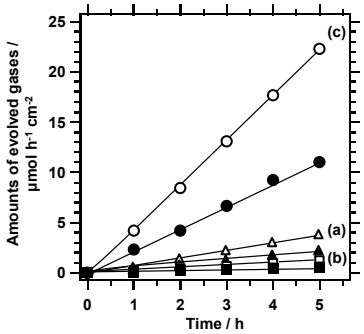

Fig. 8. Time courses of Z-scheme water splitting using photocatalyst sheets and powder suspension consisting of $SrTiO_3$:La,Rh and $BiVO_4$ under visible light ($\lambda > 420$ nm) modified with a Ru cocatalyst by photodeposition. (a) Powder suspension, (b) photocatalyst sheet without a Au layer, and (c) photocatalyst sheet with a Au layer. Open and closed symbols stand for hydrogen and oxygen, respectively.

SUMMARY AND FUTURE PROSPECTS

Recent advances in the study of the photocatalytic water splitting using particulate semiconductors were introduced. $LaMg_{1/3}Ta_{2/3}O_2N$ has been developed as an oxynitride photocatalyst for overall water splitting under irradiation at wavelengths of up to 600 nm, primarily through bandgap tuning via solid solution formation and kinetic control based on surface modifications. Surface coating with an amorphous oxide thin layer has been found to effectively suppress the self-oxidation of the oxynitride and the reverse reaction, enabling overall water splitting. The wavelength of photons usable for the overall water splitting based on one-step excitation has been extended to 600 nm; however, the apparent quantum efficiency remains low, with a value of 0.2% at 440 nm. In addition, photocatalyst sheets consisting of HEP and OEP particles embedded in a conductive layer have also been developed for efficient and scalable Z-scheme water splitting. A $SrTiO_3$:La,Rh/Au/$BiVO_4$ photocatalyst sheet splits pure water efficiently without any additives or external power supply. This superior performance is possible because electrons are transferred from the $BiVO_4$ to the $SrTiO_3$:La,Rh via the Au layer that rigidly holds the photocatalyst particles, and because hydrogen and oxygen are generated in close proximity, on the micrometer scale. The STH energy conversion efficiency of such systems has very recently been reported to exceed 1.0%. Nevertheless, the $SrTiO_3$:La,Rh and $BiVO_4$ used in these photocatalyst sheets utilize photons with wavelengths of only up to 520 and 540 nm, respectively. These short absorption edge wavelengths will continue to limit the potential of photocatalyst sheets for effective STH conversion.

The quantum efficiency of photocatalysts with long absorption edge wavelengths in water splitting has typically been low because of the low energy of their excited states, and so it is critically important to activate narrow bandgap materials to allow the practical development of solar hydrogen production by photocatalytic water splitting. In fact, there are some interesting oxynitride and oxysulfide photocatalysts with longer absorption edge wavelengths than $LaMg_{1/3}Ta_{2/3}O_2N$; $BaTaO_2N$[31], $BaNbO_2N$[32] and $La_5Ti_2Cu_{0.9}Ag_{0.1}S_5O_7$ [33] absorb visible light at wavelengths of up to 660, 730 and 710 nm, respectively. The challenges to activate such materials will remain important for progress in the field of photocatalytic water splitting. Cooperative studies related to the development of both materials and devices based on experimental and theoretical aspects will be desirable in the future study.

REFERENCES

[1] Pinaud, B. A., Benck, J. D., Seitz, L. C., Forman, A. J., Chen, Z., Deutsch, T. G., James, B. D., Baum, K. N., Baum, G. N., Ardo, S., Wang, H., Millere, E. & Jaramillo T. F. *Energy Environ. Sci.,* 6, 1983-2002 (2013).
[2] Kudo, A., Miseki, Y., *Chem. Soc. Rev*. 38, 253-278 (2009).
[3] Osterloh, F. E., *Chem. Mater.*, 20, 35-54 (2008).
[4] Kato, H., Asakura, K., Kudo, A., *J. Am. Chem. Soc*. 125, 3082-3089 (2003).
[5] Sakata, Y., Hayashi, T., Yasunaga, R., Yanaga N., Imamura, H., *Chem. Commun.*, 51, 12935-12938 (2015).
[6] Ham, Y., Hisatomi, T., Goto, Y., Moriya, Y., Sakata, Y., Yamakata, A., Kubota, J., Domen, K., *J. Mater. Chem., A*, 4, 3027-3033 (2016).

[7] Maeda, K., Takata, T., Hara, M., Saito, N., Inoue, Y., Kobayashi, H., Domen, K., *J. Am. Chem. Soc.,* 127, 8286-8287 (2005).
[8] Maeda, K., Domen, K., *J. Phys. Chem. C*, 111, 7851-7861 (2007).
[9] Hitoki, G., Takata, T., Kondo, J. N., Hara, M., Kobayashi, H., Domen, K., *Chem. Commun.,* 1698-1699 (2002).
[10] Hitoki, G., Ishikawa, A., Takata, T., Kondo, J. N., Hara, M., Domen, K., *Chem. Lett.,* 31, 736-737 (2002).
[11] Kasahara A, Nukumizu K, Hitoki G, Takata T, Kondo J N, Hara M, Kobayashi H, Domen, K., *J. Phys. Chem. A,* 106, 6750-6753 (2002).
[12] Pan, C., Takata, T., Nakabayashi, M., Matsumoto, T., Shibata, N., Ikuhara, Y., Domen, K., *Angew. Chem. Int. Ed.*, 54, 2955-2959 (2015).
[13] Pan, C., Takata, T., Domen, K., *Chem. Eur. J.*, 22, 1854-1862 (2016).
[14] Pan, C., Takata, T. Kumamoto, K., Ma, S. S. K., Ueda, K., Minegishi, T., Nakabayashi, M., Matsumoto, T., Shibata, N., Ikuhara, Y., Domen, K., *J. Mater. Chem. A*, 4, 4544-4552 (2016).
[15] Günther, E., Hagenmayer, R., Jansen, M., *Z. Anorg. Allg. Chem.*, 626, 1519-1525 (2000).
[16] Kim, Y., Woodward, P., *J. Solid State Chem.*, 180, 2798-2807 (2007).
[17] Kim, Y., Woodward, P., *J. Solid State Chem.*, 180, 3224-3233 (2007).
[18] Takata, T., Pan, C., Nakabayashi. M., Shibata, N., Domen, K., *J. Am. Chem. Soc*., 137, 9627-9637 (2015).
[19] Hisatomi, T., Kubota, J., Domen, K., *Chem. Soc. Rev.*, 43, 7520–7235 (2014).
[20] Maeda, K., *ACS Catal.*, 3, 1486−1503 (2013).
[21] Tabata, M., Maeda, K., Higashi, M., Lu, D., Takata, T., Abe, R., Domen, K., *Langmuir*, 26, 9161–9165 (2010).
[22] Maeda, K., Higashi, M., Lu, D., Abe, R., Domen, K., *J. Am. Chem. Soc*., 132, 5858–5868 (2010).
[23] Kato, H., Sasaki, Y., Shirakura, N., Kudo, A., *J. Mater. Chem. A*, 1, 12327–12333 (2013).
[24] Kato, T., Hakari, Y., Ikeda, S., Jia, Q., Iwase, A., Kudo, A., *J. Phys. Chem. Lett.*, 6, 1042–1047 (2015).
[25] Sasaki, Y., Nemoto, H., Saito, K., Kudo, A., *J. Phys. Chem. C*, 113, 17536–17542 (2009).
[26] Ma, S. S. K., Maeda, K., Hisatomi, T., Tabata, M., Kudo, A., Domen, K., *Chem. Eur. J.*, 19, 7480–7486 (2013).
[27] Jia, Q., Iwase, A., Kudo, A., *Chem. Sci.*, 5, 1513–1519 (2014).
[28] Wang, Q., Li Y., Hisatomi, T., Nakabayashi, M., Shibata, N., Kubota, J., Domen, K., *J. Catal.*, 328, 308–315 (2015).
[29] Minegishi, T., Nishimura, N., Kubota, J., Domen, K., *Chem. Sci.*, 4, 1120–1124 (2013).
[30] Wang, Q., Hisatomi, T., Jia, Q., Tokudome, H., Zhong, M., Wang, C., Pan, Z., Takata, T., Nakabayashi, M., Shibata, N., Li, Y., Sharp, I. D., Kudo, A., Yamada, T., Domen, K., *Nat. Mater.,* 15, 611-615 (2016).
[31] Ueda, K., Minegishi, T., Clune, J., Nakabayashi, M., Hisatomi, T., Nishiyama, H., Katayama, M., Shibata, N., Kubota, J., Yamada, T., Domen, K., *J. Am. Chem. Soc.*, 137, 2227−2230 (2015).
[32] Hisatomi, T., Katayama, C., Moriya, Y., Minegishi, T., Katayama, M., Nishiyama, H., Yamada, T., Domen, K., *Energy Environ. Sci.*, 6, 3595–3599 (2013).
[33] Hisatomi, T., Okamura, S., Liu, J., Shinohara, Y., Ueda, K., Higashi, T., Katayama, M., Minegishi, T., Domen, K., *Energy Environ. Sci.*, 8, 3354-3362 (2015).